HHS Public Access

Author manuscript

Clin Cancer Res. Author manuscript; available in PMC 2024 January 05.

Published in final edited form as:

Clin Cancer Res. 2023 July 05; 29(13): 2501–2512. doi:10.1158/1078-0432.CCR-22-3496.

Increased Nerve Density Adversely Affects Outcome in Oral Cancer

Cindy Perez-Pacheco[1,*], **Ligia B. Schmitd**[1,*], **Allison Furgal**[2], **Emily L. Bellile**[2], **Min Liu**[1], **Aya Fattah**[1], **Laura Gonzalez-Maldonado**[1], **Shelby P. Unsworth**[3], **Sunny Y. Wong**[3], **Laura S. Rozek**[4], **Arvind Rao**[2,5,7], **Gregory T. Wolf**[6], **Jeremy M. G. Taylor**[2,7], **Keith Casper**[6], **Michelle Mierzwa**[7], **Nisha J. D'Silva**[1,8,9]

[1]Periodontics and Oral Medicine, University of Michigan School of Dentistry, 1011 N. University Ave, Ann Arbor, MI, USA.

[2]Biostatistics, University of Michigan School of Public Health, 1415 Washington Heights, Ann Arbor, MI, USA

[3]Dermatology, University of Michigan, 1500 E Medical Center Dr, Ann Arbor, MI, USA

[4]Department of Oncology, Georgetown Lombardi Comprehensive Cancer Center, Washington DC

[5]Department of Computational Medicine & Bioinformatics, University of Michigan, Ann Arbor, MI, 48103, USA.

[6]Otolaryngology, University of Michigan Medical School, 1500 E Medical Center Dr, Ann Arbor, MI, USA.

[7]Radiation Oncology, University of Michigan Medical School, 1500 E Medical Center Dr, Ann Arbor, MI, USA.

[8]Pathology, University of Michigan Medical School, 1500 E Medical Center Dr, Ann Arbor, MI, USA.

[9]Rogel Cancer Center, University of Michigan, 1500 E Medical Center Dr, Ann Arbor, MI, USA

Abstract

Purpose: Perineural invasion (PNI) in oral cavity cancer (OSCC) is associated with poor survival. Due to the risk of recurrence, patients with PNI receive additional therapies after surgical

Correspondence should be addressed to: Nisha J D'Silva, Department of Periodontics and Oral Medicine, University of Michigan School of Dentistry, 1011 North University Ave, Room G018, Ann Arbor, MI 48109-1078, USA, Phone: (734)764-1543, Fax: (734)764-2469, njdsilva@umich.edu.

Authors' Contributions:

LBS and CPP are co-first authors. Both designed and performed experiments, analyzed and interpreted data, and wrote the manuscript. ML designed, optimized and assisted with CAM-DRG experiment. SPU and SYW provided training and guidelines for the denervation mouse experiment. AR assessed the artificial intelligence tool development and validation, and provided expertise and feedback. Aya Fattah and LGM assisted in the artificial intelligence validation. AF, ELB and JMGT performed statistics for clinical data provided expertise and feedback. KC, MM, LR, and GTW collected clinical data and provided expertise and feedback. NJD designed experiments, interpreted data, wrote the manuscript and is the guarantor of this work; has full access to all the data in the study and takes responsibility for the integrity of the data and the accuracy of the data analysis. All authors approved the final manuscript.

*These authors contributed equally.

Conflict of interest: The authors have declared that no conflict of interest exists.

resection. Mechanistic studies have shown that nerves in the tumor microenvironment promote aggressive tumor growth. Therefore, in this study, we evaluated if nerve density (ND) influences tumor growth and patient survival. Moreover, we assessed the reliability of artificial intelligence (AI) in evaluating ND.

Experimental design: To investigate if increased ND in OSCC influences patient outcome, we performed survival analyses. Tissue sections of OSCC from 142 patients were stained with hematoxylin and eosin and immunohistochemical stains to detect nerves and tumor. ND within the tumor bulk and in the adjacent 2 mm was quantified; normalized ND (NND; bulk ND/adjacent ND) was calculated. The impact of ND on tumor growth was evaluated in chick chorioallantoic-dorsal root ganglia (CAM-DRG) and murine surgical denervation models. Cancer cells were grafted and tumor size quantified. Automated nerve detection, applying the Halo-AI™ platform, was compared with manual assessment.

Results: Disease-specific-survival decreased with higher intratumoral ND and NND in tongue SCC. Moreover, NND was associated with worst-pattern-of-invasion and PNI. Increasing the number of DRG, in the CAM-DRG model, increased tumor size. Reduction of ND by denervation in a murine model, decreased tumor growth. Automated and manual detection of nerves showed high concordance with a F-1 score of 0.977.

Conclusions: High ND enhances tumor growth; and NND is an important prognostic factor that could influence treatment selection for aggressive OSCC.

Translational relevance

Identification of cancer-specific neural phenotypes associated with poor survival have the potential to improve treatment selection. Perineural invasion is associated with poor outcomes and is studied extensively. Other more easily detectable nerve-related phenotypes could also be relevant to clinical outcome. Therefore, it is important to explore these parameters. In this study, we investigated if nerve density in the tumor is linked to clinical outcome. We demonstrate that high normalized nerve density, i.e. nerve density adjusted by site, is associated with poor survival in patients with tongue cancer. Moreover, in vivo investigations support that high nerve density enhances tumor growth. Comparing normalized nerve density with other nerve-related parameters revealed associations with survival that could be relevant for treatment selection.

Keywords

nerve tissue; oral squamous cell carcinoma; tumor microenvironment

Introduction

Nerves are critical members of the tumor microenvironment significantly facilitating tumor progression. Nerves release neuropeptides (1), neurotransmitters (2–4), and growth factors to modulate cancer cells, which reciprocate by secreting neurotrophic factors that increase innervation. For example, nerve-released galanin activates galanin receptor 2 (GALR2 or GALN2) on cancer cells to induce transcriptional changes that release factors to promote cancer invasion, and enhance axonogenesis (1). Moreover, cancer cells release exosomes containing a rich cargo capable of reprogramming neurons (5) and inducing nerve growth (5,

6). Preclinical studies showed that surgical and chemical denervation suppress tumor growth (7–9), suggesting that nerves have a significant role in nurturing tumors. The dynamic communication between nerves and cancer cells occurs in multiple cancers, including head and neck, gastric, pancreatic, prostate, and breast cancers (6–10). The role of nerves in cancer development and progression may be related to the type of nerve; adrenergic nerves enhance cancer cell survival to promote tumor initiation, whereas cholinergic fibers participate in later stages of tumor progression, including invasion, migration, and metastasis (7).

Although strong evidence supports a neural influence in cancer, these findings have not yet significantly impacted diagnosis or targeted treatment selection. Perineural invasion (PNI) is currently deemed the most important neural phenotype and consequently, the focus of multiple investigations. PNI is a histopathologic feature defined as “tumor in close proximity to nerve and involving at least 33% of its circumference or tumor cells within any of the 3 layers of the nerve sheath” (11). In multiple cancers, PNI is associated with aggressive tumors and poor survival (12–19). Even prior to PNI, interactions between cancer and nerves in the tumor microenvironment could impact treatment selection and clinical outcome (12, 20). Consequently, it is essential to investigate other nerve-related parameters that reflect the biology of nerves in the tumor microenvironment. Studies have associated the presence of nerves with poor patient survival in pancreatic, esophageal and breast cancer (18, 21, 22).

Since cancer-released factors induce nerve growth and nerves modulate the tumor microenvironment, nerve density in the tumor may influence tumor progression. Nerve density is the quantification of nerves in tissue, and is increased in tumor stroma via axonogenesis, neurogenesis, and neurotropism (23). High nerve density has been associated with poor clinical outcomes in oral, prostate, and colorectal cancers (5, 7, 10, 24), however, these observations reflect only adrenergic and cholinergic innervation, and lack details on how nerve density was assessed. In this study, we investigated the impact of nerve density on survival and tumor growth in oral cavity squamous cell carcinoma (OSCC) from 142 patients, and *in vivo* models. To facilitate clinical application, we also compared artificial intelligence (AI)-based detection of nerves to manual assessment. Our findings show that high nerve density enhances tumor growth and decreases survival and could serve as an important biomarker for aggressive tumors.

Materials and Methods

Patient population

Tissue sections from 142 patients with OSCC were obtained from the Tissue Core of the University of Michigan Head and Neck Cancer Specialized Program of Research Excellence (HNSPORE)/ Head and Neck Oncology Program (HNOP). The study was conducted in accordance with good clinical practice and the Declaration of Helsinki. Institutional Review Board approval was obtained by the HNSPORE/ HNOP. All patients provided written, informed consent before study participation. The cohort was described previously (20). Briefly, tissue specimens and data were collected between 2008 and 2014, and data were updated in 2021. Data collection and immunohistochemical (IHC) stains were performed in two phases due to tissue availability. For each phase, OSCC sections from 71 patients,

here named cohorts one and two, were studied. Gender distribution of the combined cohorts was 73 males and 69 females, with a mean age of 62.8 years. Demographic, clinical and histopathologic characteristics have been published (20).

Immunohistochemistry

For human tissue, 5 μm serial sections were stained with hematoxylin and eosin (H&E), anti-S100 (Dako Omnis GA50461–2, 1:2) to highlight nerves, and anti-cytokeratin AE1/AE3 (EMD Millipore, IHCR2025–6, 1:6) to highlight epithelium. Mouse (X0931) or rabbit IgG (X0936, both Dako) served as negative controls (2 μg/mL). Mouse tissue sections were stained with H&E and S100. IHC methods were as described (20).

Data collection

Stained slides were scanned with iScan Coreo (Ventana Medical Systems, Roche Diagnostics International, Switzerland) and images analyzed with Halo Image analysis platform v3.1 (IndicaLabs), and Ventana Image Viewer software v. 3.1.4. Using cytokeratin-stained sections, two distinct adjacent areas were identified in all specimens: tumor bulk, containing tumor islands and tumor stroma; and tumor-adjacent stroma, defined as a 2 mm margin around the tumor front that contains no tumor cells (Fig. 1A). Using S100-stained sections, all nerves larger than ~10 μm in diameter were identified in the tumor bulk and adjacent stroma. No other stromal element was marked. Number and area of nerves were quantified. Contiguous nerve segments were counted as one nerve trunk. A board certified Oral and Maxillofacial Pathologist identified tumor differentiation using H&E-stained sections. PNI was scored (positive or negative) using IHC and H&E sections, following current criteria (11). Cytokeratin-stained sections were used to determine worst pattern-of-invasion (25), and to locate tumor in association with nerves to score PNI. Collection of histopathologic data was blind, without knowledge of demographics, treatment, or clinical outcome.

Nerve density is the number or area of nerve segments divided by tissue area. Intratumoral nerve density (5) and tumor-adjacent nerve density (T-AND) are number of nerve segments or total area of nerves per mm^2, in the tumor bulk or tumor-adjacent stroma, respectively (Fig. 1A). Normalized nerve density (NND) in each patient was calculated, dividing IND by T-AND.

Analysis of IND for all oral cavity sites was comprised of 142 patients. Analysis of NND included 133 patients; 9 were excluded due to lack of adjacent stromal margin around the tumor bulk. For tongue SCC, 77 patients were analyzed for IND and NND.

Artificial intelligence neural network training and assessment

Using the Halo AI™ platform (version 3.3.2541.345), we built a classifier to distinguish nerves from non-nerve tissue on S100-stained sections. A cohort of 24 tongue SCC patient samples with diverse examples of tissue background and nerve morphology, were selected. A classifier using a DenseNet AI V2 tool was built with 5695 nerve and 1963 background examples. The classifier was set to identify nerves with area ≥ 96 μm^2, which was the area from the smallest nerve considered for manual analysis. Resolution of one μm/pixel and

probability threshold of 80% were used. The cohort was split into three groups for validation of the AI classifier; 17 cases were randomly assigned into the training group, 3 into the validation group, and 4 into the test set. The training set was run for as many iterations as needed to achieve convergence for the result metrics with values above 0.99 in the validation set. These metrics were: nerve and background recall, precision, and F1 scores. Recall or sensitivity is the number of positive cases the classifier correctly predicted over all of the positive cases in the dataset. Precision or positive predictive value is a measurement of how many of the positive predictions are correct, i.e. true positives. F1 score takes into consideration both recall and precision, defined as 2*(precision*recall/precision+recall) (26). We also verified training quality by constant low cross-entropy values below 0.1. After validation, training was stopped and the classifier was run on the test set.

Cell culture

UM-SCC-1 cells (from Dr. T. Carey, University of Michigan, genotyped at our laboratory) were used in the chick chorioallantoic-dorsal root ganglia (CAM-DRG) model. MOC1 cells (from Dr. R. Uppaluri, Dana-Farber Cancer Institute, Boston) were used in mouse tumor grafts. Both cell lines were cultured in DMEM (Gibco, #11965–092) supplemented with 10% FBS (Gibco, #10082–147) and 1% Penicillin/Streptomycin (Gibco, #15140–122). Prior to subcutaneous injection, MOC1 cells (1×10^6) were resuspended in 100 μL of basement membrane matrix (Corning Matrigel, # 356234) at 5 mg/mL.

Chorioallantoic membrane-dorsal root ganglia model

The CAM-DRG model (1) was used to investigate the impact of nerve density on tumor progression. Experiments using animals were done in accordance with Institutional Animal Care and Use Committee rules from our institution. In this *in vivo* model, DRG and cancer cells were grafted onto the CAM as described (1, 27). For investigation of nerve density, one or three DRG were grafted on the upper CAM at post-fertilization day 8. UM-SCC-1 human OSCC cells were labeled with a green lipophilic dye (CellTracker Green CMFDA, Life Technologies, #C7025) for 1h, and grafted at 0.5 million cells in 5 μL on day 10, ~2 mm away from DRG. In the group with three DRG, cancer cells were placed in the center of the ‘triangle’ formed by DRG. At day 14, upper CAMs were harvested, fixed in 4% paraformaldehyde for 4h, then imaged using a stereo microscope (Nikon, SMZ1270); fixed exposure parameters were used for both groups. Tumor area in this *in vivo* method was assessed as area of fluorescence using FIJI (NIH, v.1.52; analyze particles tool). The same image threshold parameters were used in both groups.

Mouse denervation

Animal work was approved and performed at the School of Dentistry of the University of Michigan according to the guidelines of the Institutional Animal Care and Use Committee. C57BL/6J were surgically denervated as described (28, 29). Dorsal subcutaneous denervation was performed on the left side, while the right side received sham surgery. Ten days post-surgery, mice were tested for denervation by pricking the overlying skin. MOC1 mouse OSCC cells were injected subcutaneously bilaterally at a density of 1×10^6 cells in 100 μL of basement membrane matrix (Corning® growth-factor reduced Matrigel®, BD Biosciences, #354230) diluted to 5 mg/mL. Tumor growth for up to 66 days, was

monitored twice per week, and mice were euthanized when tumors reached the End-Stage Illness Scoring System established by University of Michigan Laboratory Unit for Animal Medicine (ULAM). Tumors with overlying skin were fixed in 4% paraformaldehyde for 24h. Tissues were grossed at 3 mm intervals, embedded in paraffin, and sectioned at 5μm thickness for H&E and S100 immunostaining; slides were digitally scanned for image analysis. All sections containing tumor were assessed for the number and area of nerve segments; all nerves within the tumor bulk area and within 500 μm from the tumor were quantified for each specimen. All specimens contained a stromal margin. Data from two independent experiments were pooled for analysis.

Statistics

Descriptive statistics were calculated to describe the patient sample. Disease-specific survival (DSS) was defined using the time of diagnosis as baseline. DSS probability within groups was estimated by Kaplan-Meier methods and differences between groups were examined with log-rank tests. Cox regression models were used to assess associations between patient-level characteristics and survival after adjusting for covariates. Cox models were run in SAS software version 9.4 (SAS Institute Inc., Cary, NC).

A linear mixed model of denervated:control tumor volume ratio was fit to investigate the differences in tumor growth. The linear mixed model for log2 (tumor volume) contains fixed effects for batches of mice, days, side (denervated vs control), days*side, and accounts for serial correlations over time for each tumor (autoregressive), and a random effect for each mouse.

Data Availability

The data generated in this study are available upon reasonable request to the corresponding author.

Results

High intratumoral nerve density associates with poor survival

Our previous work demonstrated that nerves in proximity to tumor islands or cells are relevant for survival (12, 20). Moreover, among nerves close to tumor, larger nerves predict poor DSS (20). This prompted us to investigate if the relative quantity of intratumoral nerves (within tumor bulk) influences clinical outcome. Nerve density was defined as the number or area of nerves/mm^2 in the tumor bulk (intratumoral nerve density, IND), or in the tumor-adjacent stroma (tumor-adjacent nerve density, T-AND) (Fig. 1A). High IND, measured using area and number of nerves in 142 OSCC patients, show a trend to diminish DSS (Fig. 1B – 1C). High, medium, and low nerve densities were defined by splitting density into tertiles. Of note, IND is usually smaller than corresponding T-AND; only 10.5% of the patients (n = 14) had IND higher than T-AND using number, and 15% (n = 20) using area of nerves.

OSCC arises at different sites in the oral cavity, also noted in our cohort of 142 patients. Tumors in the tongue were the most common (57.7%), followed by gingiva (13.4%),

floor-of-mouth (12%), and retromolar area (8.8%), with 9.1% of the regions unspecified or missing. To investigate if nerve density varies by anatomic site, we quantified IND and T-AND using number of nerves at five different intraoral sites (Fig. 1D–E). Both IND (Fig. 1D) and T-AND (Fig. 1E) were greater in the tongue compared to other sites, as expected because this region has inherently more innervation (30). Similar findings were observed with area of nerves (Supplementary Fig. 1A–B). Furthermore, patients with tongue SCC had a trend towards poor survival (Supplementary Fig. 1C).

These data suggest that although IND is meaningful to predict survival, variations in innervation across different sites in the oral cavity could influence IND. Therefore, we determined the ratio of IND to T-AND for 133 patients; nine patients were excluded due to lack of tumor-adjacent stromal margin. This normalized nerve density (NND = IND/T-AND, Fig. 1A), measured by either number or area of nerves, is equivalent across five sites (Fig. 1F–G), suggesting that this normalization method abrogates anatomical differences. Consequently, NND was used to investigate survival. First, to understand the importance of nerve density across different oral cavity sites, we plotted NND versus DSS for floor-of-mouth and gingiva (Supplementary Fig. 1D–G). No clear trend was observed between nerve density and survival for floor-of-mouth and gingiva, likely due to small patient number (n = 13 and 18, respectively). Therefore, our subsequent findings are restricted to tongue SCC.

In tongue SCC, survival of patients with high IND using number or area of nerves, was significantly poorer than those with low IND (Fig. 2A–B). Patients were split by tertiles of IND. However, no clear trend was observed for the medium IND group (red curves), which behaved similar to high IND (Fig. 2A) or low IND groups (Fig. 2B). However, when using normalized nerve density, or NND, we saw a stepwise decrease in DSS from low to high NND (Fig. 2C–D), likely because adjusting to T-AND within each patient accounts for individual variability. Thus, the use of NND may be important even when analyzing patients with OSCC at the same site.

Adjusted Cox modeling of DSS (Fig. 2E and Supplementary Table S1) showed significantly high hazard ratios associated with increased IND and NND in the tongue. Analysis is adjusted for AJCC stage (7^{th} edition), differentiation, and comorbidities. When adjusting the analysis with 8^{th} edition AJCC stage, although hazard ratios were high for increased IND and NND, only NND by number of nerves remained significant (Supplementary Table S2). Overall, these results demonstrate the strong relationship between NND and survival in tongue SCC.

To identify a clinically-relevant threshold of nerve density that associates with poor survival, we separated tongue SCC patients with NND ≥1 due to the higher IND compared to T-AND. These were only 7 or 8 patients, by number and area of nerves, respectively (Supplementary Fig. 2A–B). Patients with NND ≥1 survived significantly poorer compared to patients with lower NND. This indicates that having IND higher than T-AND is predictive of poor survival in tongue SCC. However, in multivariate analysis (adjusted for 7^{th} edition AJCC stage, differentiation, and comorbidities), although the hazard of disease-specific death is higher for patients with NND ≥1, this is not statistically significant (Supplementary Table

S3). Similar results were found when adjusting to AJCC stage 8th edition (Supplementary Table S4).

Normalized nerve density associates with pattern of invasion and perineural invasion

To understand the relationship between nerve density and other clinical and microscopic parameters used as prognostic markers in OSCC, we assessed the association between NND and differentiation status, AJCC stage (7th and 8th editions), worst pattern-of-invasion (25), and PNI. NND did not associate with either tumor differentiation (Supplementary Fig. 3A–B) or clinical stage (Supplementary Fig. 3C–F). The only significant difference was in the comparison between AJCC 8th edition stage I vs IV patients, when using area of nerves for NND (p=0.028, not shown). However, high worst pattern-of-invasion was significantly associated with high NND (Supplementary Fig. 3G–H). Tumors with worst pattern-of-invasion 4 and 5 had significantly higher NND by number and area of nerves. Worst pattern-of-invasion 4 is characterized by small islands and strands of tumor cells (25). Worst pattern-of-invasion 5 has tumor islands or cells more than 1 mm from the tumor bulk (25). Both these patterns denote aggressive phenotypes. PNI-positive patients had significantly higher NND, measured using number (Supplementary Fig. 3I), and area (Supplementary Fig. 3J) of nerves.

Since AJCC 8th edition classification incorporates depth of invasion (DOI), we explored correlations between DOI and nerve-related parameters, i.e., IND, NND, and nerve-tumor distance in tongue SCC (Supplementary Fig. 4). There were significant weak positive correlations between DOI and IND and DOI and NND by area of nerves (Supplementary Fig. 4C–D). A weak negative correlation was observed between minimum nerve-tumor distance and DOI (Supplementary Fig. 4E). These data suggest that tongue tumors with high DOI have increased nerve density and have nerves closer to tumor.

Nerve density is associated with other adverse neural phenotypes

In previous studies, we identified nerve diameter and nerve-tumor distance as predictors of prognosis (12, 20). To visualize all nerve-related parameters together, we generated multidimensional plots of NND by number and area of nerves (Fig. 3A). Besides NND (y axis) and minimum nerve-tumor distance (x axis), these plots show maximum nerve diameter in the tumor bulk (symbol size), and PNI status of each patient (triangle vs circle shape). Nerve diameter is higher in PNI-positive patients and not correlated with NND. As expected, minimum nerve-tumor distance is highly associated with PNI-positivity. However, patients with high NND were PNI-positive or -negative. This may indicate that high NND may be a better indicator of poor survival compared to PNI. Notably, it is difficult to separate the relative importance of these nerve-related parameters, since they are somewhat interdependent. For that, we plotted survival curves of NND splitting the samples into high vs low NND and minimum nerve-tumor distance (Fig. 3B–C), maximum nerve diameter (Fig. 3D–E), and PNI (Fig. 3F–G). High NND was based on the tertiles used in Fig. 2 (>0.42 for number and >0.37 for area). Regression-tree methods were used to calculate the cut-offs for minimum nerve-tumor distance (low; <27.63μm) and maximum nerve diameter (high; >26.39μm).

We previously showed that minimum nerve-tumor distance <27μm predicts poor survival in a cohort of 142 OSCC patients (20). Now we show that tongue SCC patients with high NND and low nerve-tumor distance survive poorly compared to patients with only low nerve-tumor distance (blue vs black curves in Fig. 3B and C; p=0.066 for B and p=0.026 for C). Similarly, high maximum nerve diameter in the tumor bulk was previously associated with poor DSS (20). Here, patients with high NND and high nerve diameter (green curves in Fig. 3D and E) have a trend towards poor survival compared with tongue SCC presenting only high nerve diameter (red curves, p=0.238 for D and p=0.129 for E). These data demonstrate the additive value of nerve density over other predictors of DSS.

PNI-positive patients have poor survival compared to PNI-negative ones; here we show that patients with high NND are PNI-positive or -negative (Fig. 3A). To understand how NND can help predict survival among PNI-positive and -negative patients, we split the population into four groups (Fig. 3F–G). PNI-negative patients with high NND (blue curves) have a trend towards poor survival compared to PNI-negative ones with low NND (black curves, p=0.104 for F and p=0.405 for G). Similarly, PNI-positive patients with high NND have poorer DSS (Fig. 3F–G, green curves) compared to PNI-positive, low NND (red curves; p=0.160 for F and p=0.011 for G).

Overall, these data demonstrate that NND helps predict poor survival, in addition to other established nerve-related parameters.

Artificial intelligence-based detection of nerves mimics manual detection.

Our results show the importance of different measurements of nerve density as predictors of poor prognosis in tongue SCC. However, density analysis requires assessment of all nerves (number or area) within and adjacent to the tumor, which could constrain clinical application. To overcome this limitation, we used the Halo AI™ platform to classify nerves in tissue sections and compare it to manual nerve detection. To build the nerve classifier, we trained a neural network to identify nerves stained with S100 using 17 patient samples (2818 nerves and 1190 non-nerve examples; Fig. 4A–B). This classifier was run on three validation samples and four test samples independent of the training set; parameters analyzed were precision, recall, and F1 score (Table 1). Nerve recall, precision, and F1 score were close to 1, demonstrating high accuracy of the AI-based nerve detection compared to manual annotations. This indicates AI methods have potential to streamline nerve density assessment for clinical use.

High nerve density increases tumor growth

To verify if nerve density associates with tumor growth, we used *in vivo* models. Using the chick CAM-DRG *in vivo* model (1), we grafted one or three rat DRG onto the CAM. Two days later, we grafted UM-SCC-1 cells equidistant from each DRG (Fig 5A). Four days later, CAMs were harvested for assessment of tumor area. Tumors grafted with three DRG grew significantly larger than those with one DRG (Fig. 5B), suggesting a causal relationship between nerve density and tumor growth.

In a complementary *in vivo* approach, we used a subcutaneous surgical denervation model in C57BL/6J mice (28, 29). Each mouse was denervated unilaterally with sham surgery on

the contralateral side. Equal number of MOC1 cancer cells were injected bilaterally (Fig. 5C). Overall, denervation led to significantly smaller tumors as noted in the volume ratio of tumors on the denervated to sham surgery (innervated) sides (Fig. 5D, n=16, p=0.003). To verify innervation and the success of denervation, tissue sections were stained with anti-S100, a nerve marker (Fig. 5E). As expected, denervated tumors showed fewer nerves (mean 83.2 nerves; SD 61.2) than the contralateral control tumors (mean 121.1 nerves; SD 35.3; p=0.06); the average area of nerves in denervated tumors was significantly smaller compared to control tumors (0.87 vs 1.74 mm^2, respectively; p=0.002). These data were consistent with surgical denervation, which removes larger nerves but does not completely denervate. The nerve area on the denervated side was strongly correlated with the slope of tumor volume ratio (Fig. 5F, p=0.004), while there was no correlation on the control side (Fig. 5G, p=0.91). Additionally, mice in which denervated tumors grew more than control tumors had significantly higher nerve area (Fig. 5H). These data indicate that the larger the nerves on the denervated side, the less the difference in tumor volume between both sides, suggesting that ‘denervated’ tumors maintain growth capacity if large nerves are not completely removed or regenerated. Overall, these data suggest that denervation-mediated reduction in tumor growth is nerve density-dependent.

Discussion

The present study reveals that high IND associates with poor DSS and is a strong prognostic factor in tongue cancer. These findings are supported by two different in vivo approaches; mouse surgical denervation and CAM-DRG models. Together, these findings show that high nerve density enhances tumor growth and associates with poor patient survival. Importantly, this study shows that AI/deep learning-based nerve assessment could replace manual quantification, underscoring the clinical applicability of this parameter.

The oral cavity includes different anatomic structures such as lips, tongue, palate, cheeks, and teeth that synergize to perform multiple functions. Each site’s innervation varies in quantity and quality with the structure’s function. For example, consistent with its important role in diverse functions such as taste, sensation, mastication, etc., the tongue has a complex neural network (31). In fact, innervated by five different nerves, including hypoglossal, vagus, facial, lingual, and glossopharyngeal nerves, the tongue exhibits the highest innervation in the oral cavity (30). Conversely, the buccal mucosa with a less complex function of protecting deeper tissues, has simpler innervation from the buccal nerve, a branch of the mandibular division of the trigeminal nerve (30). Because of the variability in innervation by anatomic site, IND was adjusted to T-AND, obtaining a normalized nerve density, or NND. Analysis of the three most prevalent sites of oral SCC, suggested that NND is less important for DSS for cancers of the floor-of-mouth (n = 13) and gingiva (n = 18), compared to tongue (n = 77). This could indicate that nerve density is not meaningful for all sites, or simply reflects the limitation of restricted sample size in floor-of-mouth and gingiva SCC. Interestingly, in tongue SCC, both IND and NND were significantly associated with poor DSS. However, NND better replicated biological behavior, with a stepwise increase in NND associated with a stepwise decrease in survival. Furthermore, survival of patients with NND ≥1 was strikingly poor, compared with NND <1, for both number and area of nerves. Using NND enables objective and unbiased

comparison between samples from different patients with tongue SCC. To the best of our knowledge, this is the first time that NND has been reported as a prognostic marker in oral squamous cell carcinoma.

The term tumor innervation is used interchangeably with nerve density. Most studies define nerve density as the number (9, 32–34) or area (7, 34–36) of nerve segments divided by a specific area, using tissue sections stained with H&E (5), or immunolabeled with generic or type-specific neuronal markers. Protein gene product (PGP) 9.5 antibody is commonly used to identify nerves; however, it stains parenchyma in some cancers (37, 38). In this study, we used S100 (2, 12, 32), which stains Schwann cells surrounding the axons, to count and measure area of nerve segments. Subsequently, IND and T-AND were calculated based on number or area of nerves in the tumor bulk and tumor-adjacent stromal margin, respectively. Although studies calculate nerve density differently (23), high IND has been associated with poor survival in head and neck (5), prostate (24), breast (22, 35) and colorectal (11) cancers. Similarly, our data show that tongue SCC patients with high IND have decreased DSS. Furthermore, ours is the first study showing the value of high NND for patient outcome. One study in OSCC showed poorer overall survival in patients with increased nerve density (5). However, a comparison with this study is challenging due to considerable differences in methods. Of note, survival data and histological tissue sections were extracted from the cancer genome atlas (TCGA), and authors analyzed H&E-stained sections to count nerve segments and calculate density (5).

Most of our cohort had higher T-AND compared to IND. However, the small group of patients with IND ≥ T-AND had significantly poorer survival compared to patients who presented higher T-AND than IND. In thyroid cancer, papillary tumors have almost double the nerve density of normal thyroid tissues, and IND is often higher than T-AND. In these patients, high nerve density is independently associated with extracapsular extension, a prognostic indicator of poor survival (36). Similarly, in prostate cancer nerve density is increased within the tumor compared to peripheral tissue (24); high nerve density is associated with extracapsular extension, a poor prognostic factor, and recurrence (24). Although most studies show that high IND is related to poor clinical outcome, the specific thresholds of IND vary across studies and diseases. Nerve density may be tumor-type specific; studies with standardized analysis in various tumors are required to verify this.

Since our data show that patients with high NND survive poorly, we investigated if nerve density influences tumor growth. Our complementary in vivo studies show that reduced nerve density inhibits tumor growth in mice, whereas increased nerve density promotes tumor growth in the CAM. The presence of nerves in the tumor microenvironment is very common, so it is important to understand which types of nerves are relevant for tumor growth. Only a few in vivo studies highlight the role of nerve type in tumor progression. For example, surgical ablation of sensory innervation decreases the size of tongue tumors in mice that received orthotopic xenografts of p53 null cancer cells (5). Similarly, chemical and surgical denervation of adrenergic nerves inhibits tumor initiation in mouse prostate glands (7). When adrenergic nerve receptors were genetically ablated, mice developed smaller tumors compared to wild type mice (7). Similarly, denervation of sympathetic nerves suppresses tumor growth and progression of breast cancer in mice (35). In pancreatic cancer,

contradictory results have been reported. In one study, chemical ablation of sympathetic nerves in mouse pancreas increased tumor growth suggesting that the sympathetic nervous system has an anti-tumoral function in mice with pancreatic ductal adenocarcinoma (PDAC) (39), whereas another study showed that inhibition of sympathetic nerves reduced tumor volume and improved survival in mice with PDAC (2). Moreover, an increased population of intratumoral macrophages was observed in sympathetic nerve-ablated tumors, which correlated to worse mouse survival (39).

Among nerve-cancer interactions, PNI is the most well-recognized phenotype and its diagnosis has been associated with poor survival in several cancers (12, 18–20, 40, 41). We recently showed that PNI, nerve-tumor distance, and nerve diameter in the tumor bulk are prognostic factors in oral cancer (20). Here we investigated the correlation of NND and these other nerve-related parameters in tongue SCC. Although tongue tumors with PNI have higher NND, this is not a consistent observation. We have observed that in PNI-negative patients, the presence of high NND decreased survival. Consequently, some patients could be undertreated due to the absence of PNI in their tumors despite presenting with high NND. Conversely, we identified PNI-positive patients who have low NND and survive better, for whom less aggressive treatment could potentially be an option. Since nerve-released factors modulate the tumor microenvironment to facilitate tumor development, progression, and invasion, the increase in intratumoral nerves may be more meaningful for patient survival than PNI. This is particularly important since PNI-positive nerves are rare within the entire nerve population (20). Our data support that in addition to PNI, NND should be considered an important nerve-related prognostic parameter.

Manual quantification of all nerves within the tumor bulk and tumor-adjacent stroma is a laborious task on routine histologic stains. However, recent technological advances have allowed digitization and subsequent access to AI for analysis of histopathological slides. Deep learning is a powerful and flexible method that combines large datasets and learning patterns via iterative processing and algorithmic training. Here we used an AI classifier tool to assess number and area of nerves in digitized tissue slides. Interestingly, detection of number and area of nerves obtained by automated computation have a high accuracy with the manual assessment. This evidence supports the robustness of AI-based nerve detection, overcoming the time-consuming process inherent in manual nerve density calculations, and facilitating clinical application. It is important to build a classifier with enough examples to represent the variability in morphology and staining intensity of nerves.

AI benefits have been tested in diagnosis and morphometric analysis. Visual PNI detection by pathologists and a deep learning tool had similar results for H&E-stained prostate cancer biopsies (42). Similarly, in colorectal, prostate, and pancreatic cancers, AI-based and manual PNI detection using H&E-stained sections, have acceptable agreement (43). Furthermore, automated peripheral nerve histomorphometry shows high agreement with manual morphometry, with the added advantage that automated procedures require a fraction (2.5%) of the time needed for manual methods (44). Schilling et al. shows accuracy of 87.5% in diagnosis of aganglionic megacolon (Hirschsprung’s disease; absence of ganglionic cells in the enteric nervous system) using AI-based approaches (45).

In conclusion, nerve density is a promising parameter in tongue SCC for predicting aggressive tumor behavior and could be valuable for treatment selection. Validation studies are recommended to verify the importance of nerve density in OSCC. For these studies, we recommend: 1) the use of immunohistochemistry to highlight nerves; 2) analysis of nerves in tumor and adjacent stroma; 3) calculation of normalized nerve density based on number and area of nerves/area unit.

Supplementary Material

Refer to Web version on PubMed Central for supplementary material.

Acknowledgements:

The authors thank the many investigators in the University of Michigan HNSPORE/ HNOP for their contributions to patient recruitment, assistance in data collection, and encouragement including Carol R. Bradford, MD, Thomas E. Carey, PhD, Douglas B. Chepeha, MD, Sonia Duffy, PhD, Avraham Eisbruch, MD, Joseph Helman, DDS, Kelly M. Malloy, MD, Jonathan McHugh, MD, Scott A. McLean, MD, Tamara H. Miller, RN, Jeff Moyer, MD, Mark E. Prince, MD, Nancy Rogers, RN, Matthew E. Spector, MD, Nancy E. Wallace, RN, Heather Walline, PhD, Brent Ward, DDS, and Francis Worden, MD. We greatly thank patients and their families who tirelessly participated in survey and specimen collections in the University of Michigan HNSPORE/ HNOP. The authors also thank Lisa Peterson, MPH of the University of Michigan HNSPORE/ HNOP; and Ms. Theresa Cody for excellent tissue sectioning. Support was provided by NIH/NIDCR DE027551 (N.J. D'Silva), NIH/NCI R01 CA250214 (N.J. D'Silva, L.S. Rozek), UM School of Dentistry Department of Periodontics and Oral Medicine Clinical Research Grant (N.J. D'Silva), UM CEW+ Riecker Graduate Student Research Fund (L.B. Schmitd), National Institutes of Health Grant CA46592 (E.L. Bellile and J.M.G. Taylor). UM Precision Health Investigators Award (A. Rao, L.S. Rozek), Rogel Cancer Center Support grant from the NIH/NCI P30CA046592 (A. Rao), NIH/NCI R21CA267941 (S.Y. Wong) and American Cancer Society Grant RSG-18-065-01-TBG (S.Y. Wong).

Authors' Disclosures:

C. Perez-Pacheco reports grants from NIH/NICDR DE027551 (N.J. D'Silva) during the conduct of the study. L.B. Schmitd reports grants from NIH/NIDCR DE027551 (N.J. D'Silva) and the University of Michigan CEW Riecker Graduate Student Research Fund during the conduct of the study. L. Gonzalez-Maldonado reports grants from NIH/NICDR DE027551 (N.J. D'Silva) during the conduct of the study. A. Rao reports grants from NCI Rogel Center during the conduct of the study as well as grants from NIH, NSF, DoD, and University of Michigan Ann Arbor and other support from Google Cloud, Voxel Analytics, LLC, and Genophyll, LLC outside the submitted work; in addition, A. Rao serves as member for Voxel Analytics, LLC. J.M.G. Taylor reports grants from NIH during the conduct of the study. N.J. D'Silva reports grants from NIH/National Institute of Dental and Craniofacial Research and NIH/NCI and grants and other support from University of Michigan Rogel Cancer Center during the conduct of the study as well as nonfinancial support from Eterna Therapeutics outside the submitted work. No disclosures were reported by the other authors.

References

1. Scanlon CS, Banerjee R, Inglehart RC, Liu M, Russo N, Hariharan A, et al. Galanin modulates the neural niche to favour perineural invasion in head and neck cancer. Nat Commun. 2015;6:6885. [PubMed: 25917569]
2. Renz BW, Takahashi R, Tanaka T, Macchini M, Hayakawa Y, Dantes Z, et al. β2 Adrenergic-Neurotrophin Feedforward Loop Promotes Pancreatic Cancer. Cancer Cell. 2018;33(1):75–90.e7. [PubMed: 29249692]
3. Sarrouilhe D, Clarhaut J, Defamie N, Mesnil M. Serotonin and cancer: what is the link? Curr Mol Med. 2015;15(1):62–77. [PubMed: 25601469]
4. Lang K, Bastian P. Neurotransmitter effects on tumor cells and leukocytes. Prog Exp Tumor Res. 2007;39:99–121. [PubMed: 17314504]
5. Amit M, Takahashi H, Dragomir MP, Lindemann A, Gleber-Netto FO, Pickering CR, et al. Loss of p53 drives neuron reprogramming in head and neck cancer. Nature. 2020;578(7795):449–54. [PubMed: 32051587]

6. Madeo M, Colbert PL, Vermeer DW, Lucido CT, Cain JT, Vichaya EG, et al. Cancer exosomes induce tumor innervation. Nat Commun. 2018;9(1):4284. [PubMed: 30327461]
7. Magnon C, Hall SJ, Lin J, Xue X, Gerber L, Freedland SJ, et al. Autonomic nerve development contributes to prostate cancer progression. Science. 2013;341(6142):1236361. [PubMed: 23846904]
8. Saloman JL, Albers KM, Li D, Hartman DJ, Crawford HC, Muha EA, et al. Ablation of sensory neurons in a genetic model of pancreatic ductal adenocarcinoma slows initiation and progression of cancer. Proc Natl Acad Sci U S A. 2016;113(11):3078–83. [PubMed: 26929329]
9. Zhao CM, Hayakawa Y, Kodama Y, Muthupalani S, Westphalen CB, Andersen GT, et al. Denervation suppresses gastric tumorigenesis. Sci Transl Med. 2014;6(250):250ra115.
10. Zhao Q, Yang Y, Liang X, Du G, Liu L, Lu L, et al. The clinicopathological significance of neurogenesis in breast cancer. BMC Cancer. 2014;14:484. [PubMed: 24996968]
11. Liebig C, Ayala G, Wilks JA, Berger DH, Albo D. Perineural invasion in cancer. Cancer. 2009;115(15):3379–91. [PubMed: 19484787]
12. Schmitd LB, Beesley LJ, Russo N, Bellile EL, Inglehart RC, Liu M, et al. Redefining Perineural Invasion: Integration of Biology With Clinical Outcome. Neoplasia. 2018;20(7):657–67. [PubMed: 29800815]
13. Tai SK, Li WY, Chu PY, Chang SY, Tsai TL, Wang YF, et al. Risks and clinical implications of perineural invasion in T1–2 oral tongue squamous cell carcinoma. Head Neck. 2012;34(7):994–1001. [PubMed: 21953773]
14. Tarsitano A, Tardio ML, Marchetti C. Impact of perineural invasion as independent prognostic factor for local and regional failure in oral squamous cell carcinoma. Oral Surg Oral Med Oral Pathol Oral Radiol. 2015;119(2):221–8. [PubMed: 25487983]
15. Santoro A, Angelico G, Travaglino A, Inzani F, Arciuolo D, Valente M, et al. Prognostic role of perineural invasion in vulvar squamous cell carcinoma: A systematic review and meta-analysis. Eur J Surg Oncol. 2022.
16. Yekedüz E, Dizdar Ö, Kertmen N, Aksoy S. Comparison of Clinical and Pathological Factors Affecting Early and Late Recurrences in Patients with Operable Breast Cancer. J Clin Med. 2022;11(9).
17. Chen YF, Wang SY, Le PH, Chen TH, Kuo CJ, Lin CJ, et al. Prognostic Significance of Perineural Invasion in Patients with Stage II/III Gastric Cancer Undergoing Radical Surgery. J Pers Med. 2022;12(6).
18. Griffin N, Rowe CW, Gao F, Jobling P, Wills V, Walker MM, et al. Clinicopathological Significance of Nerves in Esophageal Cancer. Am J Pathol. 2020;190(9):1921–30. [PubMed: 32479822]
19. Delahunt B, Murray JD, Steigler A, Atkinson C, Christie D, Duchesne G, et al. Perineural invasion by prostate adenocarcinoma in needle biopsies predicts bone metastasis: Ten year data from the TROG 03.04 RADAR Trial. Histopathology. 2020;77(2):284–92. [PubMed: 32285460]
20. Schmitd LB, Perez-Pacheco C, Bellile EL, Wu W, Casper K, Mierzwa M, et al. Spatial and Transcriptomic Analysis of Perineural Invasion in Oral Cancer. Clin Cancer Res. 2022.
21. Ferdoushi A, Griffin N, Marsland M, Xu X, Faulkner S, Gao F, et al. Tumor innervation and clinical outcome in pancreatic cancer. Sci Rep. 2021;11(1):7390. [PubMed: 33795769]
22. Li D, Hu LN, Zheng SM, La T, Wei LY, Zhang XJ, et al. High nerve density in breast cancer is associated with poor patient outcome. FASEB Bioadv. 2022;4(6):391–401. [PubMed: 35664834]
23. Schmitd LB, Perez-Pacheco C, D'Silva NJ. Nerve density in cancer: Less is better. FASEB Bioadv. 2021;3(10):773–86. [PubMed: 34632313]
24. Olar A, He D, Florentin D, Ding Y, Ayala G. Biologic correlates and significance of axonogenesis in prostate cancer. Hum Pathol. 2014;45(7):1358–64. [PubMed: 24767770]
25. Brandwein-Gensler M, Teixeira MS, Lewis CM, Lee B, Rolnitzky L, Hille JJ, et al. Oral squamous cell carcinoma: histologic risk assessment, but not margin status, is strongly predictive of local disease-free and overall survival. Am J Surg Pathol. 2005;29(2):167–78. [PubMed: 15644773]
26. Singh P, Singh N, Singh KK, Singh A. Chapter 5 - Diagnosing of disease using machine learning. In: Singh KK, Elhoseny M, Singh A, Elngar AA, editors. Machine Learning and the Internet of Medical Things in Healthcare: Academic Press; 2021. p. 89–111.

27. Schmitd LB, Liu M, Scanlon CS, Banerjee R, D'Silva NJ. The Chick Chorioallantoic Membrane In Vivo Model to Assess Perineural Invasion in Head and Neck Cancer. J Vis Exp. 2019(148).
28. Peterson SC, Eberl M, Vagnozzi AN, Belkadi A, Veniaminova NA, Verhaegen ME, et al. Basal cell carcinoma preferentially arises from stem cells within hair follicle and mechanosensory niches. Cell Stem Cell. 2015;16(4):400–12. [PubMed: 25842978]
29. Peterson SC, Brownell I, Wong SY. Cutaneous Surgical Denervation: A Method for Testing the Requirement for Nerves in Mouse Models of Skin Disease. J Vis Exp. 2016(112).
30. Kamrani P, Sadiq NM. Anatomy, Head and Neck, Oral Cavity (Mouth). StatPearls. Treasure Island (FL): StatPearls Publishing Copyright © 2022, StatPearls Publishing LLC.; 2022.
31. D'Silva NJ, Perez-Pacheco C, Schmitd LB. The 3D's of Neural Phenotypes in Oral Cancer: Distance, Diameter, and Density. Adv Biol (Weinh). 2022:e2200188. [PubMed: 36373694]
32. Reeves FA, Battye S, Roth H, Peters JS, Hovens C, Costello AJ, et al. Prostatic nerve subtypes independently predict biochemical recurrence in prostate cancer. J Clin Neurosci. 2019;63:213–9. [PubMed: 30772200]
33. Ceyhan GO, Schäfer KH, Kerscher AG, Rauch U, Demir IE, Kadihasanoglu M, et al. Nerve growth factor and artemin are paracrine mediators of pancreatic neuropathy in pancreatic adenocarcinoma. Ann Surg. 2010;251(5):923–31. [PubMed: 20395845]
34. Amit M, Na'ara S, Gil Z. Mechanisms of cancer dissemination along nerves. Nat Rev Cancer. 2016;16(6):399–408. [PubMed: 27150016]
35. Kamiya A, Hayama Y, Kato S, Shimomura A, Shimomura T, Irie K, et al. Genetic manipulation of autonomic nerve fiber innervation and activity and its effect on breast cancer progression. Nature Neuroscience. 2019;22(8):1289–305. [PubMed: 31285612]
36. Ayala GE, Dai H, Powell M, Li R, Ding Y, Wheeler TM, et al. Cancer-related axonogenesis and neurogenesis in prostate cancer. Clin Cancer Res. 2008;14(23):7593–603. [PubMed: 19047084]
37. Hibi K, Westra WH, Borges M, Goodman S, Sidransky D, Jen J. PGP9.5 as a candidate tumor marker for non-small-cell lung cancer. Am J Pathol. 1999;155(3):711–5. [PubMed: 10487828]
38. Tomita T. PGP 9.5 immunocytochemical staining for pancreatic endocrine tumors. Islets. 2013;5(3):122–8. [PubMed: 23959334]
39. Guillot J, Dominici C, Lucchesi A, Nguyen HTT, Puget A, Hocine M, et al. Sympathetic axonal sprouting induces changes in macrophage populations and protects against pancreatic cancer. Nature communications. 2022;13(1):1985-.
40. Kazemian E, Solinski M, Adams W, Moore M, Thorpe EJ. The role of perineural invasion in parotid malignancy outcomes: A systematic review and meta-analysis. Oral Oncol. 2022;130:105937. [PubMed: 35662029]
41. Guo YN, Tian DP, Gong QY, Huang H, Yang P, Chen SB, et al. Perineural Invasion is a Better Prognostic Indicator than Lymphovascular Invasion and a Potential Adjuvant Therapy Indicator for pN0M0 Esophageal Squamous Cell Carcinoma. Ann Surg Oncol. 2020;27(11):4371–81. [PubMed: 32519146]
42. Kartasalo K, Ström P, Ruusuvuori P, Samaratunga H, Delahunt B, Tsuzuki T, et al. Detection of perineural invasion in prostate needle biopsies with deep neural networks. Virchows Arch. 2022;481(1):73–82. [PubMed: 35449363]
43. Park Y, Park J, Jang G-J. Efficient Perineural Invasion Detection of Histopathological Images Using U-Net. Electronics. 2022;11(10):1649.
44. Daeschler SC, Bourget M-H, Derakhshan D, Sharma V, Asenov SI, Gordon T, et al. Rapid, automated nerve histomorphometry through open-source artificial intelligence. Sci Rep. 2022;12(1):5975-. [PubMed: 35396530]
45. Schilling F, Geppert CE, Strehl J, Hartmann A, Kuerten S, Brehmer A, et al. Digital pathology imaging and computer-aided diagnostics as a novel tool for standardization of evaluation of aganglionic megacolon (Hirschsprung disease) histopathology. Cell Tissue Res. 2019;375(2):371–81. [PubMed: 30175382]

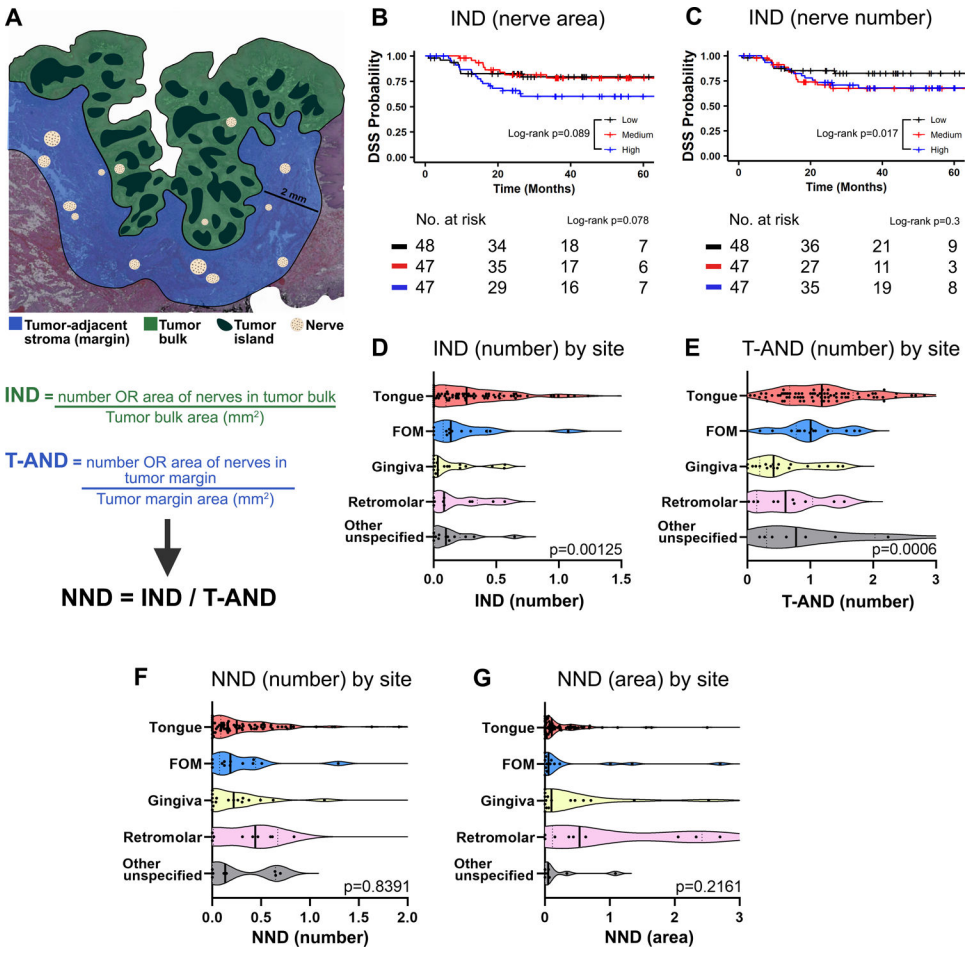

Figure 1: Intratumoral nerve density associates with poor survival in OSCC.

A, Schematic representation of zones for nerve density analysis. **B** and **C**, High intratumoral nerve density (IND) calculated using area (**B**) and number (**C**) of nerves associate with poor DSS. **D**, IND measured by number of nerves with patients grouped by tumor location. **E**, T-AND measured by number of nerves with patients grouped by tumor location. Note high IND and T-AND in tongue SCC in **D** and **E**. **F**, Normalized nerve density (NND) measured by number of nerves with patients grouped by tumor location. **G**, NND measured by area of nerves, and tumor location. **B** and **C** show Kaplan-Meier survival curves with log-rank statistics; patients are split by tertiles of IND using area (**B**), and number (**C**) of nerves. The number of patients at risk for each time point is shown below each plot. Kruskal-Wallis test was used in **D** through **G**, a few datapoints were excluded/cut from **D**-**G** plots for better visualization but all data was considered for analysis; FOM = floor-of-mouth.

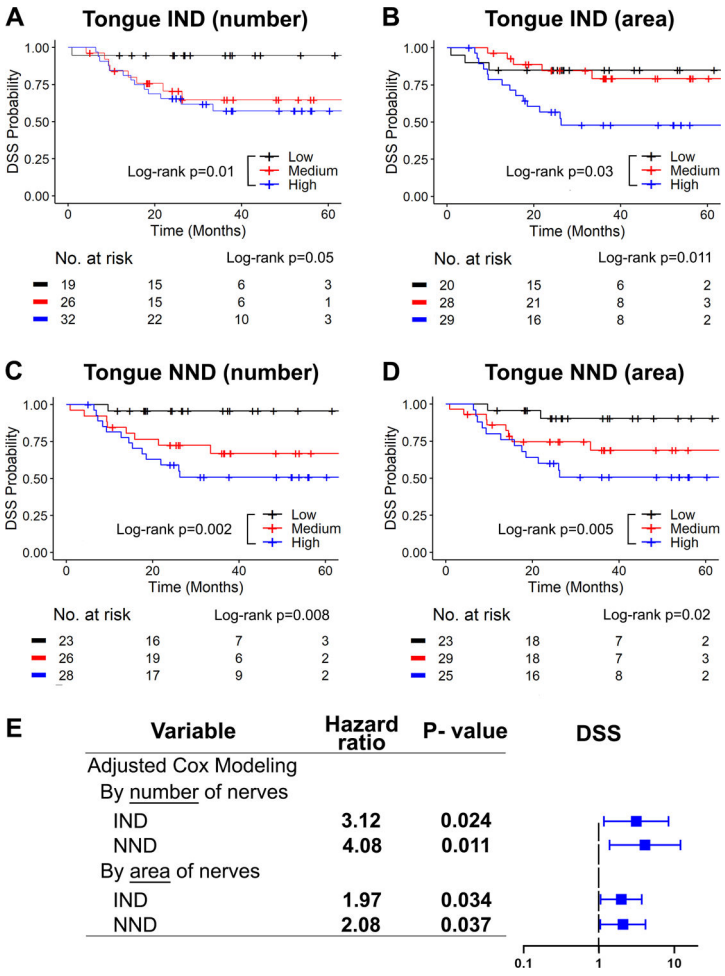

Figure 2: High normalized nerve density (IND/T-AND) independently associates with poor survival in tongue SCC.

A and **B**, High IND in the tongue associates with poor DSS, for both number (**A**) and area (**B**) of nerves. **C** and **D**, High NND in the tongue associates with poor DSS when calculated using number (**C**) and area (**D**) of nerves. Kaplan-Meier survival curves with log-rank statistics are shown in **A** through **D**; patients are split by tertiles of IND or NND and the number of patients at risk for each time point is shown below each plot. (**E**) Adjusted Cox modeling of DDS. Data is adjusted for tumor clinical stage (AJCC 7th edition), differentiation and comorbidities. Significant HRs at $p<0.05$ are shown in bold and depicted in blue. IND and NND values were log-transformed to fit the model. HR= Hazard ratio.

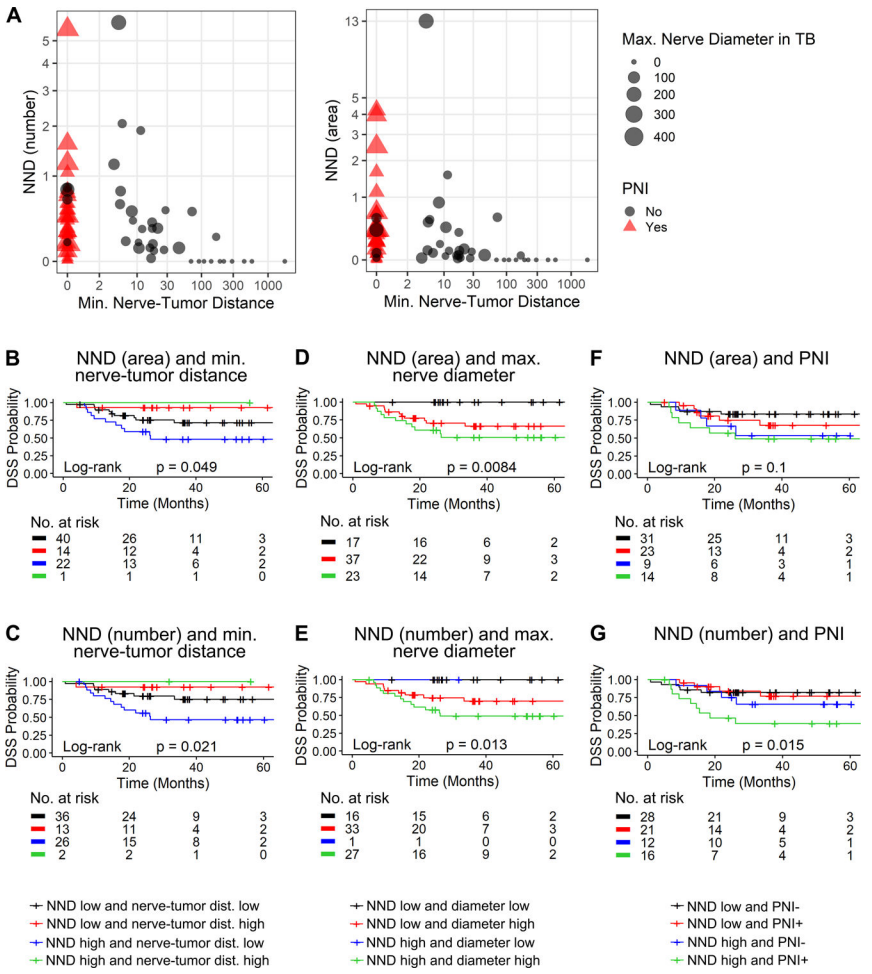

Figure 3: NND helps predict survival in association with other nerve-related parameters.

A, Multidimensional plots of NND versus minimum nerve-tumor distance, classifying patients by maximum nerve diameter in the tumor bulk and PNI status; NND measured with number (left plot) and area (right plot) of nerves. Kaplan-Meier curves of NND and other nerve-related parameters; minimum nerve-tumor distance (**B** and **C**), maximum nerve diameter in the tumor bulk, (**D** and **E**), and PNI (**F** and **G**). Overall log-rank statistics are shown within each plot in **B** through **G**; patients are split by cut-offs obtained by regression-tree analyses for nerve-tumor distance (27.63 μm) and diameter (26.39 μm). NND cut-off is defined as the high tertile of NND (0.42). The number of patients at risk for each time point is shown below each plot.

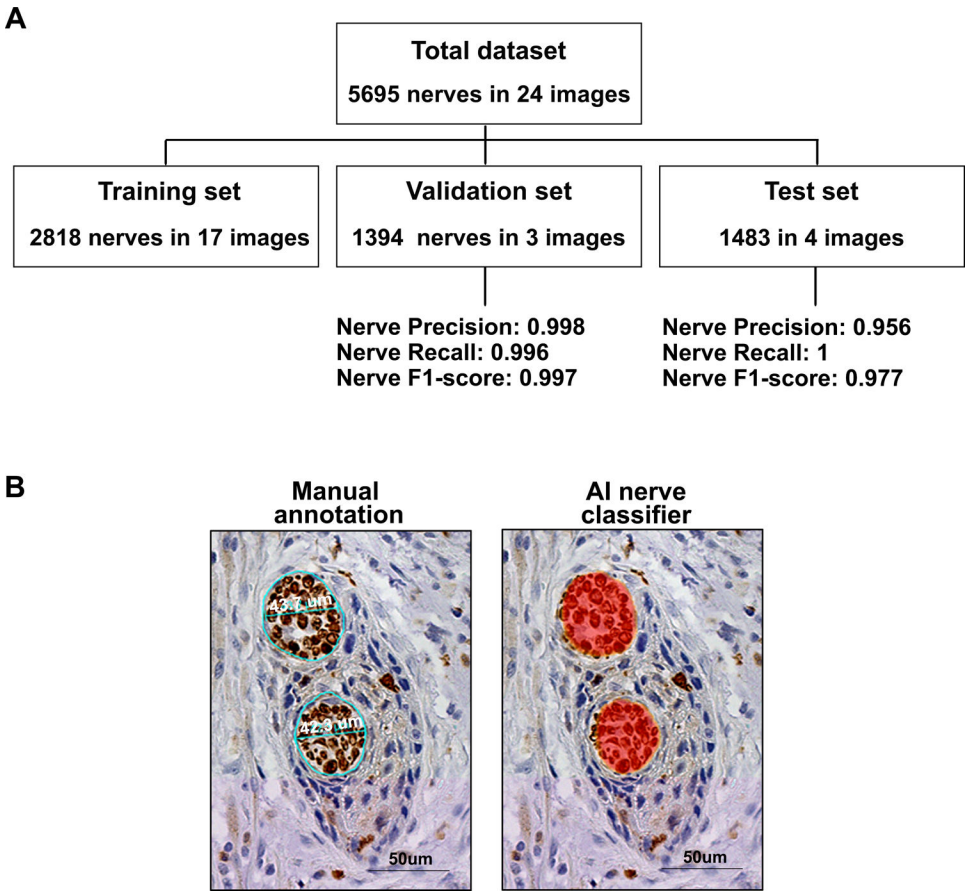

Figure 4: Artificial intelligence-based detection of nerve density replicates manual detection.

A, Flowchart of datasets. The total dataset was composed of 5695 nerves drawn in 24 images, and it was split in training, validation and test sets. Precision, recall and F1-score for detecting nerves are presented for the validation and test set. **B**, Comparison between manual annotations of nerves (Diameters of upper and lower nerves were 43.7 μm and 42.3 μm, respectively) and AI classifier mask identifying the same nerves (red overlay on the right). Bar = 50 μm

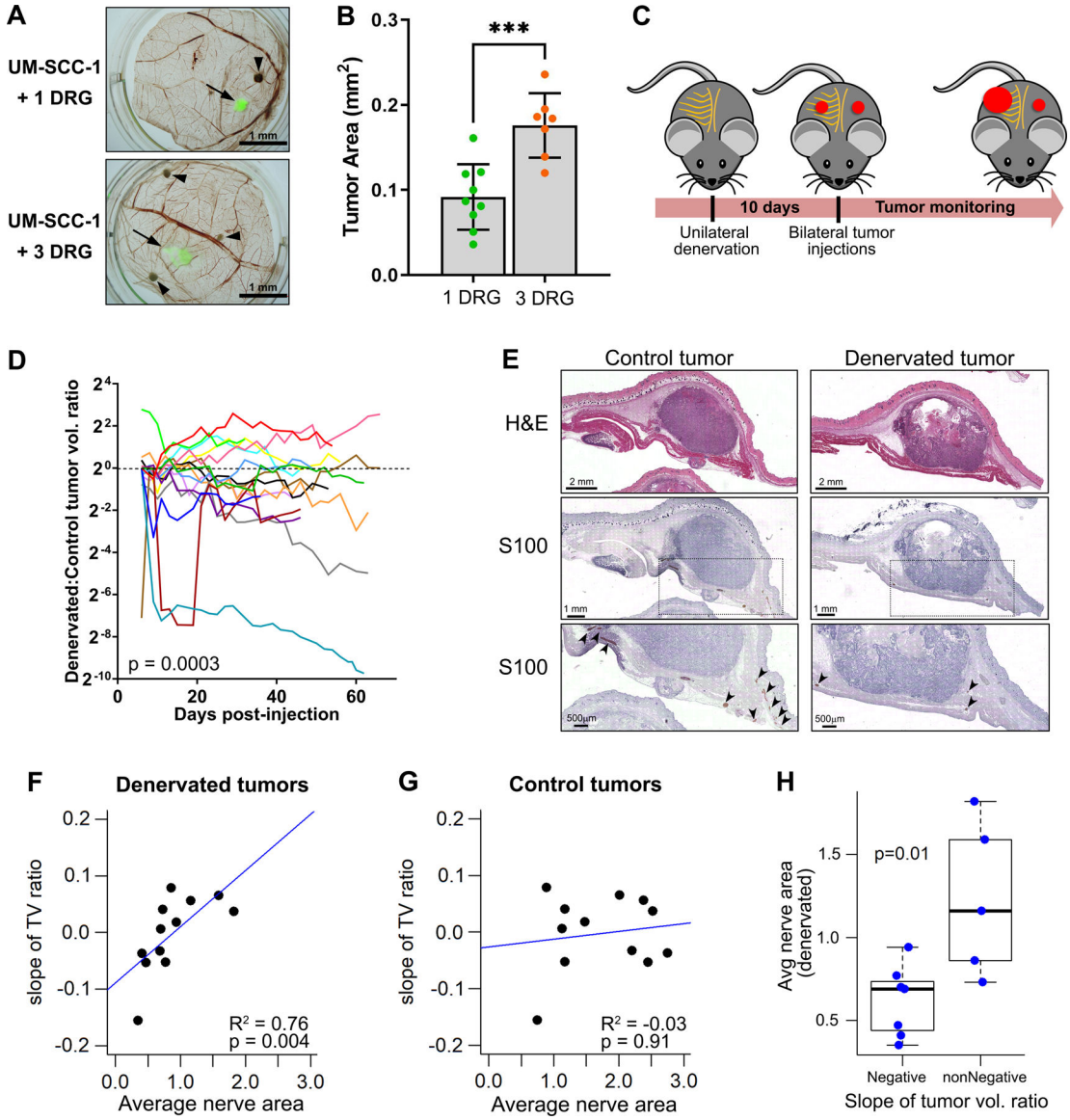

Figure 5: High nerve density increases tumor growth.

A, In vivo assessment of nerve density using the CAM-DRG model. DRGs were grafted on day 8 and fluorescently labeled UM-SCC-1 cells on day 10; upper CAMs were harvested on day 14. Arrows show labeled UM-SCC-1 cells, arrowheads show DRG locations. **B**, Tumor area quantification based on fluorescence; unpaired t-test p-value: *** <0.01. **C**, Schematic representation of surgical denervation. Subcutaneous dorsal nerves were removed unilaterally from C57BL6/J mice with sham surgery on the contralateral side. MOC1 cells were injected bilaterally after 10 days. **D**, Denervated/ control tumor volume ratio; each mouse is represented by a different color (n = 16; linear mixed model p-value = 0.0003). **E**, Histologic sections of control and denervated tumors. S100 stain facilitated nerve assessment in tissue sections. Arrows show nerve segments. **F** and **G**, Correlation between slope of tumor volume ratio and average nerve area on denervated (**F**) and control tumors (**G**). Strong positive correlation on the denervated side; Spearman

correlation coefficients p-values are shown. **H**, Average nerve area in denervated tumors versus denervated:control slope of tumor volume ratio over time. Negative slope refers to mice where denervated tumors were smaller than control; non-negative slope has opposite behavior or no differences between denervated and control (t test p-value is shown).

Table 1:

Statistical analysis of number and area of nerves comparing manual and AI assessment.

Parameter	P1	P2	P3	P4	Overall
Nerve precision (PPV)	0.908	0.998	0.961	0.955	0.956
Nerve recall (sensitivity)	1	1	1	1	1
Nerve F1-Score	0.952	0.999	0.980	0.977	0.977

P1 to P4 denote patients in the AI validation test set.

PPV denotes positive predictive value.